ACS APPLIED MATERIALS & INTERFACES

Research Article

www.acsami.org

Systematic Control of Photophysical Properties of Host Materials for High Quantum Efficiency above 25% in Green Thermally Activated Delayed Fluorescent Devices

Chil Won Lee and Jun Yeob Lee*,†

Department of Polymer Science and Engineering Dankook University, Jukjeon-dong, Suji-gu, Yongin-si, Gyeonggi-do 448-701, Republic of Korea

ABSTRACT: Three donor−acceptor type host materials with different photophysical properties were developed by managing the interconnect position of the donor and acceptor moieties and molecular structure of the host materials was correlated with the electro-optical properties and device performances of the host materials. The linkage via the meta-position of aromatic units was better than the linkage via ortho- or para-positions and high quantum efficiency of 26.0% in the green thermally activated delayed fluorescent device was achieved using the host material with the meta-linkage.

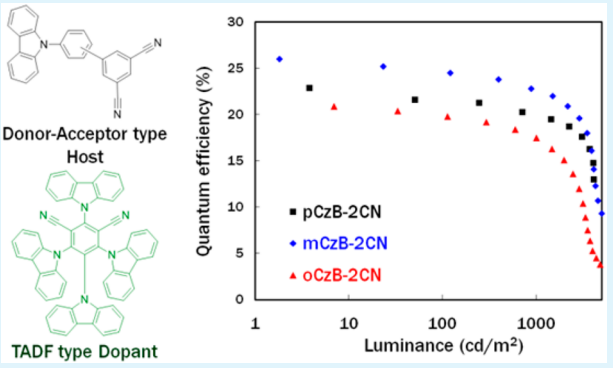

KEYWORDS: *green fluorescent device, thermally activated delayed fluorescence, donor−acceptor type host, carbazole, dicyanobenzene, high quantum efficiency*

INTRODUCTION

Thermally activated delayed fluorescent (TADF) devices have gained great interest since the first demonstration of high quantum efficiency close to 20% using a donor−acceptor type highly emissive TADF emitter.[1] Triplet harvesting by reverse intersystem crossing originated from small singlet−triplet energy gap induced the high quantum efficiency of the TADF devices.[2,3]

After the pioneering work by Adachi group about the high efficiency TADF devices, much effort has been devoted to enhance the quantum efficiency of the TADF devices.[4−6] One of the most successful approaches was to optimize carrier balance in the emitting layer using a mixed host or a bipolar host with a donor−acceptor structure. Mixed hosts possessing hole transport type hosts and electron transport type hosts were applied as the host material for the TADF dopants, and high external quantum efficiency above 25% could be demonstrated.[7,8] Similarly, bipolar hosts could provide high quantum efficiency above 20% because of optimized charge balance and activated TADF emission.[9−11] However, only a few materials have been reported as the host materials for the high quantum efficiency TADF devices and further study about the host materials for the TADF emitter is required. In particular, donor−acceptor type bipolar host materials needs to be developed.

In this work, a series of donor−acceptor type host materials with different interconnect positions between the donor and acceptor moieties, 4′-(9-carbazolyl)-[1,1′-biphenyl]-3,5-dicarbonitrile (pCzB-2CN), 3′-(9-carbazol-9-yl)-[1,1′-biphenyl]-3,5-dicarbonitrile (mCzB-2CN) and 2′-(9-carbazol-9-yl)-[1,1′-biphenyl]-3,5-dicarbonitrile (oCzB-2CN), were developed and the electro-optical properties and device performances of the host materials were investigated according to the interconnect position of the host materials. It was found that the interconnection via meta-position of aromatic unit is the most effective to improve the quantum efficiency of the TADF devices and a high external quantum efficiency of 26.0% was obtained using mCzB-2CN. This work proved that the interconnect position between the donor and acceptor units of the donor−acceptor type host materials is critical to the photophysical properties and device performances of the host materials for TADF devices.

EXPERIMENTAL SECTION

General Information. Tetrakis(triphenylphosphine)palladium(0) ($Pd(PPh_3)_4$, P&H tech) potassium carbonate and tetrahydrofuran-(THF, Duksan Chem. Co.) were used without further purification. 4-(9-Carbazolyl)phenylboronic acid, 3-(9-carbazolyl)phenylboronic acid and 5-bromoisophthalonitrile (P&H tech) were used as received. Detailed characterization of the synthesized compounds were carried out according to the method described in the literature.[12]

Synthesis. *Representative Synthesis of 4′-(9-Carbazolyl)-[1,1′-biphenyl]-3,5-dicarbonitrile (pCzB-2CN).* A solution of 4-(9-carbazolyl)phenylboronic acid (2.00 g, 7.10 mmol) and 5-bromoisophthalonitrile (1.23 g, 5.92 mmol) dissolved in THF(150 mL) was stirred

Received: November 24, 2014
Accepted: January 8, 2015
Published: January 22, 2015

DOI: 10.1021/am508259u
ACS Appl. Mater. Interfaces 2015, 7, 2899−2904

Scheme 1. Synthetic Scheme of CzB-2CN Series

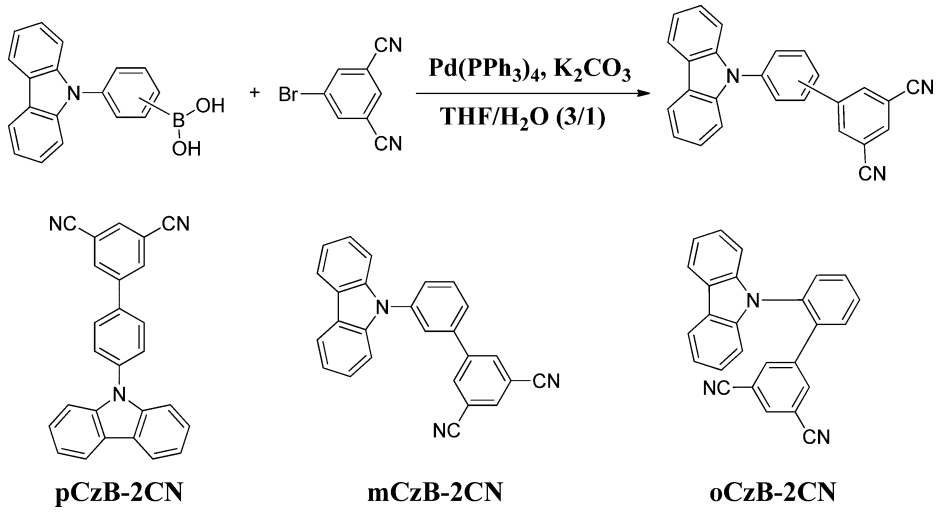

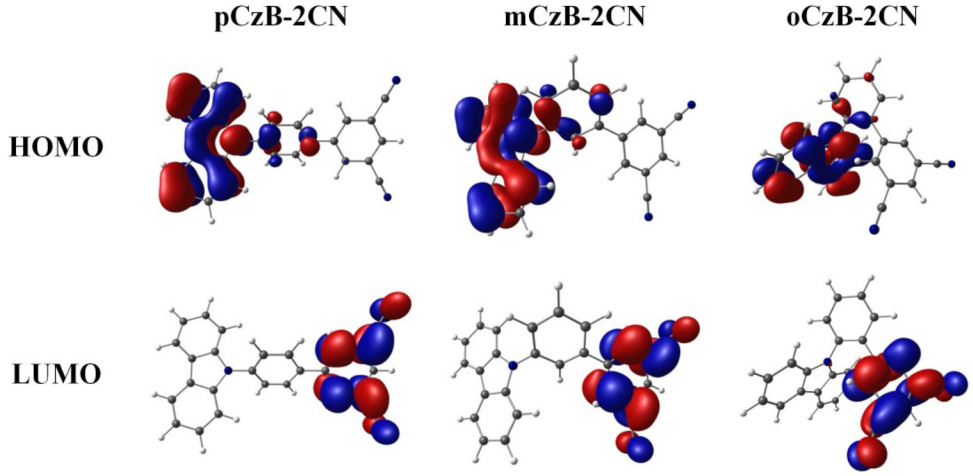

Figure 1. HOMO and LUMO distribution of CzB-2CN series.

in a double-necked flask and bubbled with nitrogen gas for 30 min. Aqueous solution of potassium carbonate (0.2 M, 50 mL) was poured in a previous solution and was bubbled for 30 min further. After adding $Pd(PPh_3)_4$ (0.34 g, 0.30 mmol) to the mixture, the resulting solution was refluxed overnight under nitrogen gas. The reaction mixture was cooled down to room temperature, extracted with ethyl acetate and distilled water. The organic layer was evaporated to remove solvent and the resulting product was purified by column chromatography from *n*-hexane/dichloromethane(1/5) to give the white pCzB-2CN crystalline product. Finally, pCzB-2CN was purified by sublimation under reduced pressure. 3′-(9-Carbazolyl)-[1,1′-biphenyl]-3,5-dicarbonitrile (mCzB-2CN) and 2′-(9-carbazolyl)-[1,1′-biphenyl]-3,5-dicarbonitrile (oCzB-2CN) were prepared using similar methods described above.

pCzB-2CN. Yield 65%. T_m 313 °C. ^{1}H NMR (500 MHz, DMSO-d_6): δ 7.33 (t, 2H, J = 4.0 Hz), 7.45−7.47 (m, 4H), 7.80 (d, 2H, J = 4.0 Hz), 8.16 (d, 2H, J = 4.0 Hz), 8.27 (d, 2H, J = 3.8 Hz), 8.49 (s, 1H), 8.67 (s, 2H). ^{13}C NMR (125 MHz, DMSO-d_6):δ 109.6, 113.6, 117.2, 120.3, 120.5, 122.9, 126.3, 127.1, 129.0, 134.8, 135.1, 137.8, 139.9, 141.3. MS (FAB) m/z 369 [M$^+$]. EA Calcd for $C_{26}H_{15}N_3$: C(84.53%), H(4.09%), N(11.37%). Found: C(84.58%), H(4.10%), N(11.38%).

mCzB-2CN. Yield 68%. T_m 267 °C. ^{1}H NMR (500 MHz, DMSO-d_6): δ 7.30 (t, 2H, J = 4.0 Hz), 7.42−7.45 (m, 4H), 7.71 (d, 1H, J = 4.0 Hz), 7.81 (t, 1H, J = 5.2 Hz), 7.99 (d, 1H, J = 4.0 Hz), 8.15 (s, 1H), 8.25 (d, 2H, J = 3.8 Hz), 8.44 (s, 1H), 8.65 (s, 2H). ^{13}C NMR (125 MHz, DMSO-d_6):δ 109.8, 113.5, 117.2, 120.2, 120.5, 122.8, 125.6, 126.3, 126.5, 127.4, 131.0, 135.0, 135.1, 137.9, 138.3, 140.1, 141.2. MS (FAB) m/z 369 [M$^+$]. EA Calcd for $C_{26}H_{15}N_3$: C(84.53%), H(4.09%), N(11.37%). Found: C(84.52%), H(4.09%), N(11.42%).

oCzB-2CN. Yield 60%. T_m 185 °C. ^{1}H NMR (400 MHz, DMSO-d_6): δ 6.96 (d, 2H, J = 3.8 Hz), 7.20 (t, 2H, J = 4.9 Hz), 7.28 (t, 2H, J = 4.9 Hz), 7.37 (s, 2H), 7.44 (s, 1H), 7.56−7.70 (m, 4H), 8.04 (d, 2H, J = 3.8 Hz). ^{13}C NMR (100 MHz, DMSO-d_6):δ 109.4, 113.8, 116.3, 120.6, 120.8, 123.3, 126.4, 129.7, 129.9, 130.6, 131.0, 131.2, 133.9, 135.2, 136.7, 140.9, 141.5. MS (FAB) m/z 369 [M$^+$]. EA Calcd for $C_{26}H_{15}N_3$: C(84.53%), H(4.09%), N(11.37%). Found: C(84.22%), H(4.08%), N(11.27%).

Device Fabrication and Measurement. Device configuration was indium tin oxide (ITO, 50 nm)/poly(3,4-ethylenedioxythiophene):poly(styrenesulfonate) (PEDOT:PSS, 60 nm)/4,4′-cyclohexylidenebis[*N*,*N*-bis(4-methylphenyl) aniline] (TAPC, 20 nm)/1,3-bis(*N*-carbazolyl)benzene (mCP, 10 nm)/host: (4s,6s)-2,4,5,6-tetra(9*H*-carbazol-9-yl)isophthalonitrile (4CzIPN, 25 nm, 5%)/diphenylphosphine oxide-4-(triphenylsilyl)phenyl (TSPO1, 35 nm)/LiF(1 nm)/Al(200 nm). A hole-only device with a device structure of ITO (50 nm)/PEDOT:PSS (60 nm)/TAPC (20 nm)/mCP (10 nm)/pCzB-2CN, mCzB-2CN or oCzB-2CN (25 nm)/TAPC (5 nm)/Al (200 nm) and an electron-only device with a device structure of ITO (50 nm)/Ca (5 nm)/ pCzB-2CN, mCzB-2CN or oCzB-2CN (25 nm)/TSPO1 (30 nm)/LiF (1 nm)/Al (200 nm) were also fabricated to compare hole and electron density. The electrical and optical performances of the CzB-2CN series OLEDs were characterized with a Keithley 2400 source measurement unit and CS1000 spectroradiometer.

DOI: 10.1021/am508259u
ACS Appl. Mater. Interfaces 2015, 7, 2899−2904

RESULTS AND DISCUSSION

The three host materials synthesized in this work, pCzB-2CN, mCzB-2CN and oCzB-2CN, possess carbazole as the donor unit and isophthalonitrile as the acceptor unit. The electron-donating and electron-withdrawing character of each unit may separate the highest occupied molecular orbital (HOMO) and the lowest unoccupied molecular orbital (LUMO), and may allow bipolar carrier transport properties and narrow HOMO−LUMO gap. In addition, the change of the interconnect position between carbazole and isophthalonitrile can control singlet and triplet energies of the host materials.

Synthetic scheme of pCzB-2CN, mCzB-2CN, and oCzB-2CN is presented in Scheme 1. The three compounds were simply synthesized by Suzuki coupling reaction between boronic acid of (9-carbazolyl)phenyl and brominated isophthalonitrile using Pd catalyst. Synthetic yield of the compounds was 65−70% after purification by vacuum train sublimation. Chemical structure of the compounds was verified by chemical analysis such as ^{1}H and ^{13}C nuclear magnetic resonance, elemental analysis, and mass analysis.

The HOMO and LUMO distribution of the host materials was studied by molecular simulation using Gaussian 09 program. B3LYP 6-31G* was a basis set for the molecular simulation and orbital distribution of the host materials is shown in Figure 1. Complete separation of the HOMO and LUMO was displayed by the donor−acceptor molecular structure of the host materials. Localization of the HOMO on the electron donating carbazole unit and dispersion of the LUMO on the electron withdrawing isophthalonitrile unit was observed.

Photoluminescence (PL) emission and ultraviolet−visible (UV−vis) absorption of pCzB-2CN, mCzB-2CN and oCzB-2CN were measured and optical spectra are presented in Figure 2. UV−vis absorption and PL spectra of the host materials were

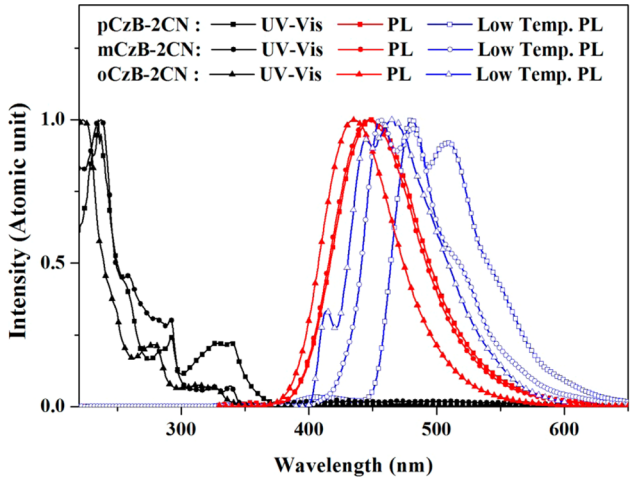

Figure 2. UV−vis and PL spectra of CzB-2CN series.

shifted to long wavelength by changing the interconnect position from ortho, meta, to para of phenyl by extended conjugation between carbazole and isophthalonitrile. Triplet energies calculated from phosphorescence spectra of pCzB-2CN, mCzB-2CN, and oCzB-2CN were 2.58, 2.73, and 2.99 eV, respectively. Disconnection of conjugation between carbazole and isophthalonitrile by the ortho-linkage increased the triplet energy of oCzB-2CN.

To confirm the shortened conjugation of the oCzB-2CN host, we identified the geometrical structure of the oCzB-2CN host by single-crystal X-ray diffraction analysis. ORTEP diagram of oCzB-2CN is shown in Figure 3. Dihedral angles of carbazole to central phenyl ring and isophthalonitrile to central phenyl ring were 88.1 and 59.5°, respectively. The carbazole moiety was almost perpendicular to the central phenyl ring by steric hindrance, which isolates the carbazole moiety and central phenyl unit. Therefore, the triplet energy of the oCzB-2CN host was high compared to that of other host materials. The large dihedral angle of the isophthalonitrile unit to the central phenyl ring is also due to steric hindrance by the ortho-substitution.

Cyclovoltammetry (CV) measurements of the host materials were carried out to determine ionization potential (IP) and electron affinity (EA) from oxidation and reduction curves (Figure 4). Oxidation/reduction potentials of pCzB-2CN, mCzB-2CN, and oCzB-2CN were 1.29/−1.59 V, 1.27/−1.62 V, and 1.35/−1.67 V, respectively. IP and EA were calculated from the oxidation and reduction potentials using ferrocene as a standard material. IP/EA of pCzB-2CN, mCzB-2CN, and oCzB-2CN were −6.09/−3.21, −6.07/−3.18, and −6.15/−3.13 eV, respectively.[13] The IP was deepened in oCzB-2CN, whereas the EA was stabilized in pCzB-2CN. Therefore, the IP-EA gap was narrow in pCzB-2CN, whereas it was wide in oCzB-2CN. The narrow IP-EA gap of pCzB-2CN is due to extended molecular structure and the wide IP-EA gap of oCzB-2CN is due to twisted molecular structure, which reduces the degree of conjugation. Even though the IP-EA gap of oCzB-2CN was 3.02 eV, pCzB-2CN and mCzB-2CN showed IP-EA gap less than 3.00 eV, which was narrower than that of other bipolar host materials because of the strong donor−acceptor character.

As the pCzB-2CN, mCzB-2CN, and oCzB-2CN compounds were developed as the host materials for TADF emitters, delayed fluorescence of TADF emitter doped host materials was analyzed. A well-known TADF emitter, 4CzIPN, was doped in the host materials for transient PL characterization. Transient PL intensity was plotted against time in Figure 5. The three host materials exhibited delayed fluorescence decay of 4CzIPN in the microsecond range, suggesting activation of TADF emission by the host materials. The relatively high triplet energy of the synthesized host materials compared to singlet (2.49 eV) and triplet energy of 4CzIPN (2.37 eV) activated the TADF emission of 4CzIPN. Excited-state lifetimes for TADF emission calculated from the transient PL decay curves were 3.6, 3.5, and 3.8 μs, which was shorter than the lifetime reported in the CBP:4CzIPN system (5.1 μs).[1] Therefore, it is anticipated that the three host materials can provide high quantum efficiency in the 4CzIPN TADF devices by activating delayed fluorescent emission through reverse intersystem crossing. PL quantum yields of 4CzIPN-doped pCzB-2CN, mCzB-2CN, and oCzB-2CN films were 0.83, 1.00, and 0.75, respectively. The relatively low PL quantum yield of the pCzB-2CN:4CzIPN film may be due to low triplet energy of pCzB-2CN, whereas the low PL quantum yield of oCzB-2CN:4CzIPN film is due to poor energy transfer in spite of high triplet energy.

The activation of delayed PL emission of 4CzIPN enabled the fabrication of the 4CzIPN TADF devices using pCzB-2CN, mCzB-2CN, and oCzB-2CN as the host materials. Device configuration was ITO (50 nm)/PEDOT:PSS (60 nm)/TAPC (20 nm)/mCP (10 nm)/host:4CzIPN (25 nm, 5%)/TSPO1

DOI: 10.1021/am508259u
ACS Appl. Mater. Interfaces 2015, 7, 2899−2904

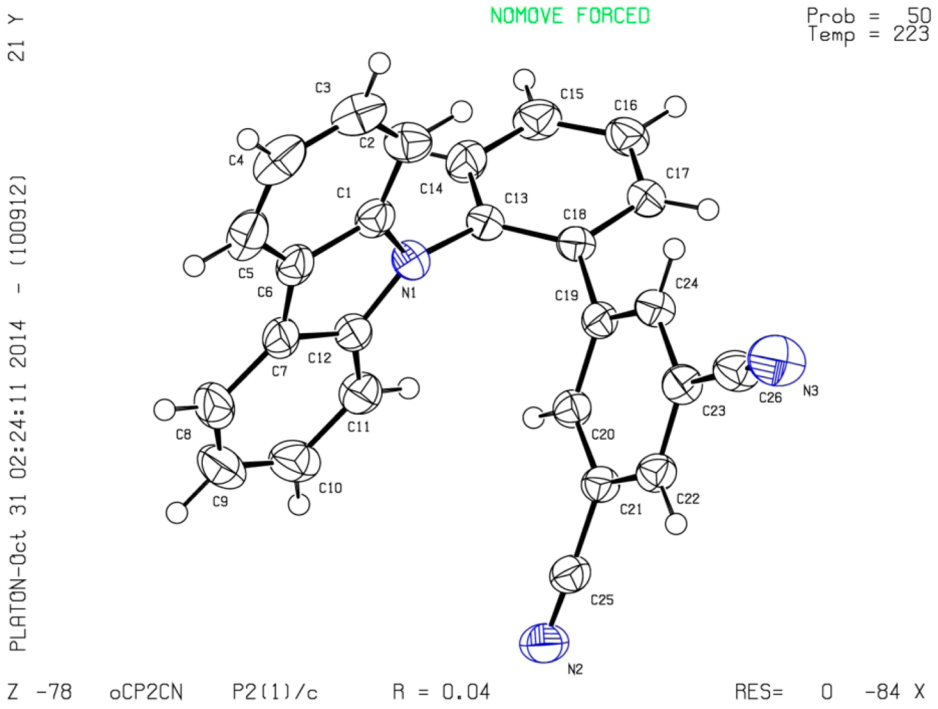

Figure 3. ORTEP diagram of oCzB-2CN.

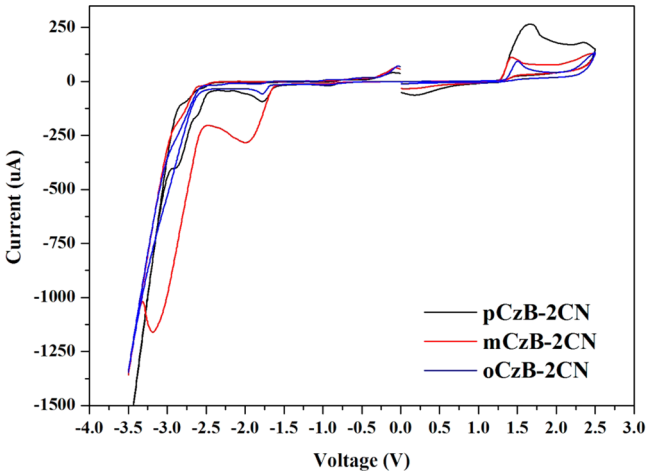

Figure 4. Cyclic voltammetry curves of CzB-2CN series.

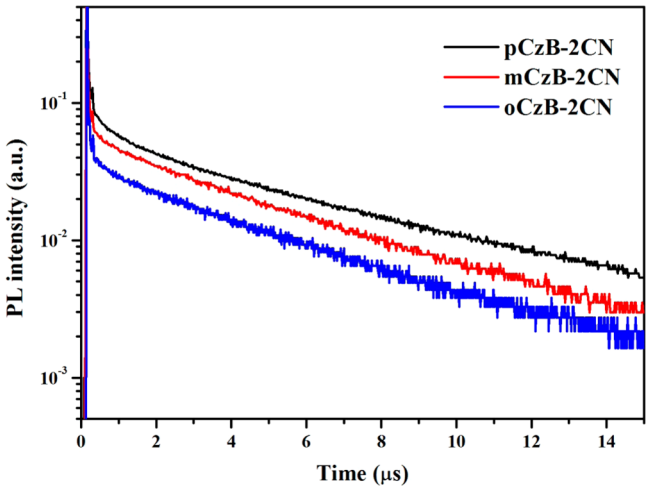

Figure 5. Transient PL decay curves of CzB-2CN series.

(35 nm)/LiF(1 nm)/Al(200 nm). Current density and luminance of the 4CzIPN devices were measured according to voltage and were plotted against driving voltage in Figure 6. The current density and luminance of the 4CzIPN devices were in the order of pCzB-2CN > mCzB-2CN > oCzB-2CN, which agreed with the order of IP-EA gap of the host materials. The extended backbone structure of pCzB-2CN facilitates charge transport by hopping between molecules via orbital overlap, increasing the current density. In the case of the oCzB-2CN, distorted backbone structure by ortho-linkage disturbs the orbital overlap between molecules, reducing the current density. The current density and luminance of mCzB-2CN host were in between those of pCzB-2CN and oCzB-2CN.

Quantum efficiency and power efficiency calculated from the current density−voltage-luminance data were presented against luminance in Figure 7. The quantum efficiency was maximized in the mCzB-2CN device and the maximum quantum efficiency was 26.0%. The quantum efficiency was 22.6% even at 1000 cd/

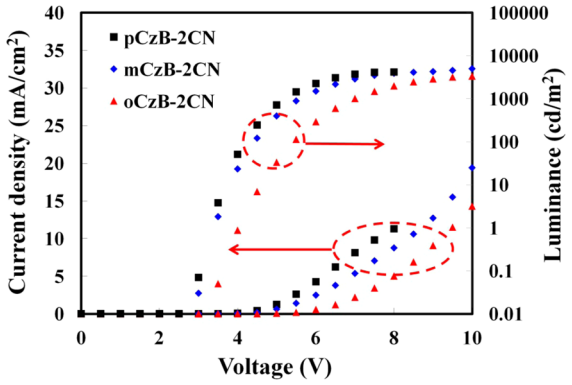

Figure 6. Current density−voltage−luminance curves of CzB-2CN series:4CzIPN devices.

DOI: 10.1021/am508259u
ACS Appl. Mater. Interfaces 2015, 7, 2899−2904

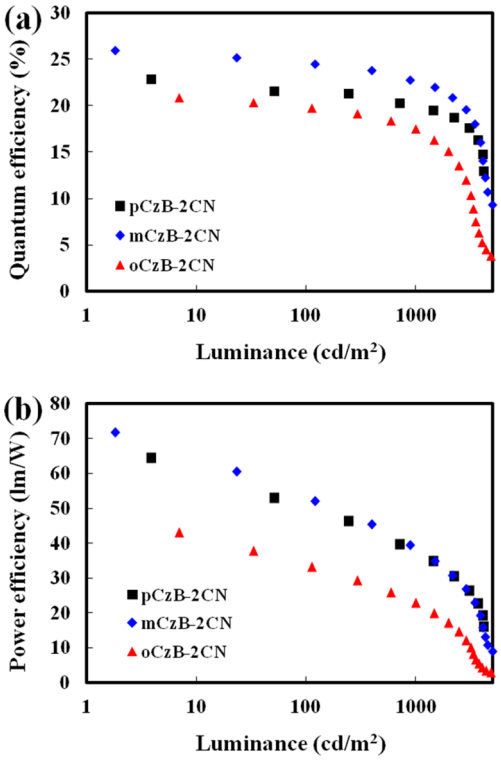

Figure 7. (a) Quantum efficiency–luminance curves and(b) power efficiency–luminance curves of CzB-2CN series:4CzIPN devices.

m^2. The quantum efficiency was degraded in the pCzB-2CN and oCzB-2CN devices and the maximum quantum efficiencies of the pCzB-2CN and oCzB-2CN devices were 22.9 and 20.9%. The high quantum efficiency of the mCzB-2CN device is due to high PL quantum yield of the 4CzIPN doped mCzB-2CN film, whereas the relatively low quantum efficiency of the pCzB-2CN and oCzB-2CN devices is due to the low PL quantum yield of the 4CzIPN-doped pCzB-2CN and oCzB-2CN films. The device quantum efficiency could be well-correlated with the PL quantum yield of the 4CzIPN-doped films. In the case of the power efficiency, the power efficiency of the pCzB-2CN and mCzB-2CN devices was similar in spite of relatively low quantum efficiency of the pCzB-2CN devices because of low driving voltage of the pCzB-2CN devices originated by narrow IP-EA gap of the host material. Maximum power efficiencies of the pCzB-2CN and mCzB-2CN devices were 71.7 and 64.4 lm/W. Although the device performances of the 4CzIPN devices were optimized in the mCzB-2CN devices, all host materials displayed high maximum quantum efficiency above 20%. Triplet harvesting by delayed fluorescence via reverse intersystem crossing of 4CzIPN resulted in the high quantum efficiency. Other than this, bipolar nature of the host by donor–acceptor structure as presented in single carrier device data (Figure 8) and carrier confinement inside the device also enhanced the quantum efficiency of the 4CzIPN TADF devices. Device performances of the 4CzIPN devices are summarized in Table 1.

Electroluminescence (EL) spectra of the 4CzIPN TADF devices are presented in Figure 9. EL emission of 4CzIPN was dependent on the host materials and red-shift of EL emission was observed in the pCzB-2CN and mCzB-2CN devices. Peak emission wavelengths were 510, 508, and 502 nm in the pCzB-2CN, mCzB-2CN and oCzB-2CN devices. The red-shift of the

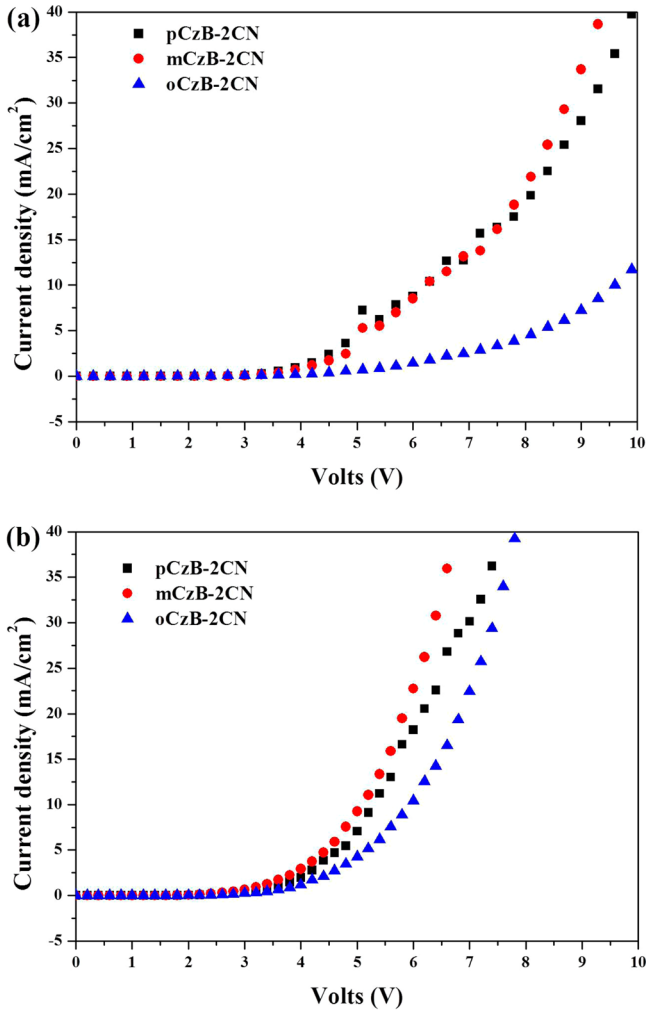

Figure 8. Current density–voltage curves of (a) hole-only and (b) electron-only devices of CzB-2CN series.

Table 1. Device Performances of CzB-2CN Series Green OLEDs

material	max. Q.E. (%)	QE (%) at 1000 nit	max PE (lm/W)	color index at 1000 nit
pCzB-2CN	22.9	19.9	64.4	0.26, 0.55
mCzB-2CN	26.0	22.5	71.7	0.24, 0.54
oCzB-2CN	20.9	17.5	46.6	0.24, 0.51

EL spectra might be due to strong dipole interaction between the host materials and 4CzIPN. Donor–acceptor structure of the host materials may induce strong intermolecular interaction, which would be significant in the pCzB-2CN with an extended molecular structure. The wavelength shift was in agreement with the degree of distortion of the backbone structure.

CONCLUSIONS

In summary, photophysical properties of donor–acceptor type host materials were systematically managed by controlling the interconnect positions between the donor and acceptor units. Low driving voltage was achieved using the pCzB-2CN host, whereas high quantum efficiency and high triplet energy were

DOI: 10.1021/am508259u
ACS Appl. Mater. Interfaces 2015, 7, 2899–2904

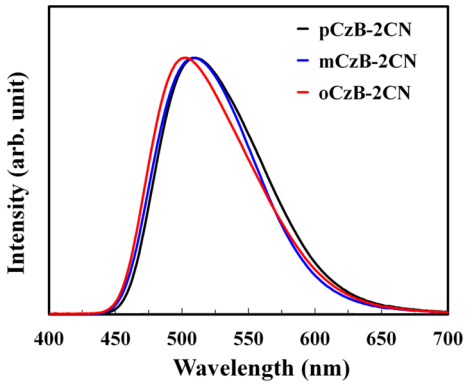

Figure 9. EL spectra of CzB-2CN series:4CzIPN devices.

obtained using the mCzB-2CN and oCzB-2CN host materials, respectively. Optimized 4CzIPN devices with the mCzB-2CN host showed high quantum efficiency of 26.0% and the donor−acceptor type design is promising for managing the photophysical properties and device performances of the TADF devices.

AUTHOR INFORMATION

Corresponding Author

*E-mail: leej17@dankook.ac.kr.

Present Address

†J.Y.L. is currently at School of Chemical Engineering, Sungkyunkwan University, 2066 Seobu-ro Jangan-gu, Suwon-si, Gyeonggi-do 440-746, Republic of Korea

Notes

The authors declare no competing financial interest.

ACKNOWLEDGMENTS

This research was supported by Basic Science Research Program through the National Research Foundation of Korea (NRF) funded by the Ministry of Education, Science and Technology (NRF-2013R1A1A2011560) and Ministry of Science, ICT and future Planning (2013R1A2A2A010674) and development of red and blue OLEDs with external quantum efficiency over 20% using delayed fluorescent materials funded by MOTIE.

REFERENCES

(1) Uoyama, H.; Goushi, K.; Shizu, K.; Nomura, H.; Adachi, C. Highly Efficient Organic Light-Emitting Diodes from Delayed Fluorescence. *Nature* **2012**, *492*, 234−238.

(2) Valeur, B. *Molecular Fluorescence: Principles and Applications*, 1st ed.; Wiley−VCH: Weinheim, Germany, 2002; pp 41−42.

(3) Dias, F. B.; Bourdakos, K. N.; Jankus, V.; Moss, K. C.; Karntekar, K. T.; Bhalla, V.; Santos, J.; Bryce, M. R.; Monkman, A. P. Triplet Harvesting with 100% Efficiency by Way of Thermally Activated Delayed Fluorescence in Charge Transfer OLED Emitters. *Adv. Mater.* **2013**, *25*, 3707−3714.

(4) Tanaka, H.; Shizu, K.; Miyazaki, H.; Adachi, C. Efficient Green Thermally Activated Delayed Fluorescence (TADF) from a Phenoxazine−Triphenyltriazine (PXZ−TRZ) Derivative. *Chem. Commun.* **2012**, *48*, 11392−11394.

(5) Zhang, Q.; Li, B.; Huang, S.; Nomura, H.; Tanaka, H.; Adachi, C. Efficient Blue Organic Light-Emitting Diodes Employing Thermally Activated Delayed Fluorescence. *Nat. Photonics* **2014**, *8*, 326−332.

(6) Wang, H.; Xie, L.; Peng, Q.; Meng, L.; Wang, Y.; Yi, Y.; Wang, P. Novel Thermally Activated Delayed Fluorescence Materials−Thioxanthone Derivatives and Their Applications for Highly Efficient OLEDs. *Adv. Mater.* **2014**, *26*, 5198−5204.

(7) Lee, S. Y.; Yasuda, T.; Nomura, H.; Adachi, C. High-Efficiency Organic Light-Emitting Diodes Utilizing Thermally Activated Delayed Fluorescence from Triazine-Based Donor−Acceptor Hybrid Molecules. *Appl. Phys. Lett.* **2012**, *101*, 093306.

(8) Kim, B. S.; Lee, J. Y. Engineering of Mixed Host for High External Quantum Efficiency above 25% in Green Thermally Activated Delayed Fluorescence Device. *Adv. Funct. Mater.* **2014**, *24*, 3970−3977.

(9) Im, Y.; Lee, J. Y. Above 20% External Quantum Efficiency in Thermally Activated Delayed Fluorescence Device Using Furodipyridine-Type Host Materials. *Chem. Mater.* **2014**, *26*, 1413−1419.

(10) Kim, B. S.; Lee, J. Y. Phosphine Oxide Type Bipolar Host Material for High Quantum Efficiency in Thermally Activated Delayed Fluorescent Device. *ACS Appl. Mater. Interfaces* **2014**, *6*, 8396−8400.

(11) Cho, Y. J.; Yook, K. S.; Lee, J. Y. A Universal Host Material for High External Quantum Efficiency Close to 25% and Long Lifetime in Green Fluorescent and Phosphorescent OLEDs. *Adv. Mater.* **2014**, *26*, 4050−4055.

(12) Lee, D. R.; Lee, C. W.; Lee, J. Y. High Triplet Energy Host Materials for Blue Phosphorescent Organic Light-Emitting Diodes Derived from Carbazole Modified Orthophenylene. *J. Mater. Chem. C* **2014**, *2*, 7256−7263.

(13) D'Andrade, B. W.; Datta, S.; Forrest, S. R.; Djurovich, P.; Polikarpov, E.; Thompson, M. E. Relationship Between The Ionization and Oxidation Potentials of Molecular Organic Semiconductors. *Org. Electron.* **2005**, *6*, 11−20.

DOI: 10.1021/am508259u
ACS Appl. Mater. Interfaces 2015, 7, 2899−2904